The cold air drainage model KLAM_21 - Model formulation and comparison with observations

U. Sievers and M. Kossmann*

Deutscher Wetterdienst, Frankfurter Strasse 135, 63067 Offenbach, Germany

**Correspondence to: Meinolf Kossmann (meinolf.kossmann@dwd.de)*

Abstract

A brief description of the physics and numerical techniques of the cold air drainage model KLAM_21 is presented. The single layer model has been developed as an environmental consultancy tool for simulations of nocturnal airflow in hilly and mountainous terrain under dry fair weather conditions. Typical model applications include frost protection (cold air ponding) and air quality (nocturnal ventilation). Basic KLAM_21 outputs are the depth and total heat deficit of the cold air layer and the layer averaged velocity and direction of the airflow. Optionally, effects of an ambient (regional) wind and/or the dispersion of a passive tracer can be simulated. Comparisons of model simulations with observations at two sites in Germany and from a case study in Christchurch (NZ) are presented for model evaluation. Good agreement between KLAM_21 simulations and observations is found for cold air layer depths, near surface winds, and spatial drainage wind patterns.

1 Introduction

Detailed knowledge of the depth, intensity and direction of nocturnal drainage wind systems is required for many aspects of environmental consultancy, such as the assessment of urban ventilation or frost risk during calm synoptic conditions (e.g. Gross, 1989; Quenol and Beltrando, 2008). Drainage winds often occur in areas with heterogeneous surface cover (agriculture, cities, forest, water). Land use related differential cooling occurs after sunset in addition to the relief generated temperature differences. This differential cooling can lead to the development of thermally induced wind systems, such as land or country breezes, which are superimposed on to the katabatic drainage winds.

Consultancy studies, e.g. about possible degradation of ventilation due to the blocking or weakening of drainage flows by a new road or railway running on a dam, or by construction of new residential or industrial areas, require airflow simulations with a spatial resolution of a few tens of meters or less, which are beyond the scope of mesoscale models. Large-eddy-simulations (LES) are able to calculate drainage flows with a high spatial resolution, but the high demand of computation time still limits the application of LES to rather small domains (Skyllingstad, 2003; Lageron et al., 2010; Trachte et al., 2010; Burns and Chemel, 2014). Therefore, simplified two-dimensional cold air drainage models have been developed in the past (e.g. Mattson and Nordbeck, 1980; Garrett and Smith, 1984; Schädler and Lohmeyer, 1994; Riether et al., 1994) to perform fast computations of drainage flows with very high resolution in large domains. Two-dimensional drainage wind models have only 1 vertical layer of variable depth for which mean wind speeds and directions are calculated. They are computationally fast, mainly because the number of

computational grid points required for a large domain with small grid spacing is low compared to a 3-dimensional model, but partly also because of inherent simplifications in the model physics.

Due to its mountainous terrain, nocturnal drainage winds are very common in New Zealand (e.g. Fitzharris et al., 1980; Wratt et al., 1984; Sturman et al. 1985; McKendry et al., 1986; McGowan and Sturman, 1993 & 1996; Corsmeier et al., 2006). For modelling studies of drainage winds in New Zealand various 3-dimensional meso-scale computer models have been used, such as RAMS (Sturman and Zawar-Reza, 2002), MM5 (Titov et al., 2007), TAPM (Zawar-Reza and Sturman, 2008; Broadbent et al. 2010, Appelhans and Zawar-Reza, 2011, Tate et al., 2011), or WRF (Powell, 2014). Running such meso-scale models successfully requires substantial education and practice. Computational costs and model parameterisations usually limit the spatial resolution to grid spacing of 500-2000 m or more. In general, mesoscale models are able to capture drainage winds at the resolved scale. But specific problems have been encountered regarding complex drainage wind patterns (Wilson and Zawar-Reza, 2006) and overestimation of drainage wind speeds (Zawar-Reza et al., 2005). Assimilation of observational data has been used to improve model results (Wilson and Zawar-Reza, 2006).

Complementary to available mesoscale models, Sievers (2005) developed the single-layer (2-dimensional) cold air drainage model KLAM_21 with simplified model–physics as a fast and easy-to-use tool to estimate the behaviour and impact of nocturnal drainage wind systems with high spatial and temporal resolution under varying environmental conditions. The computer model source code is written in FORTRAN. Currently KLAM_21 is operated on *Unix/Linux* and *Microsoft Windows* operation systems. For *Windows* operation systems a graphical user interface is available. A full description and manual of the model in German language is given by Sievers (2005). The present publication provides a citable description of the model in English language as international interest in using KLAM_21 (e.g. in USA, Wales, Canada) for research application has been growing steadily. A brief description of the basic physics and numerical techniques of KLAM_21 is given in Sections 2 and 3, while required input data and output data provided by the model are described in Section 4. Section 5 presents comparisons of simulation results with case study observations, including a model application for Christchurch (New Zealand), where multi-scale terrain features generate complex drainage wind patterns. A discussion of results and conclusions follows in Section 6.

2. Basic model physics

The single-layer cold air drainage model KLAM_21 (Kaltluft-Abfluss-Modell, developed during the first couple of years of the 21st century) calculates depth, velocity, and flow direction of a stably stratified boundary layer (cold air layer) that evolves from a neutrally stratified, dry atmosphere during nighttime over complex terrain.

2.1 Heat deficit and depth of the cold air layer

Temporal changes in the total heat deficit E of the stably stratified cold air layer are calculated from a prescribed constant local heat loss rate P (depending only on surface type, see Table 1) and horizontal advection:

$$\frac{\partial E}{\partial t} = P - \nabla_h \cdot c_p \, H \left\langle \rho_{eff} \; \bar{v}_h \; T' \right\rangle \qquad (1)$$

where H is the depth of the cold air layer (i.e. the layer with deviations from the initially assumed neutral temperature

profile) and brackets $\langle ... \rangle$ indicate vertical averaging from the height of the terrain surface above sea level h_0 to the top of the stably stratified cold air layer $h_0 + H$. $\vec{v}_h$ is the horizontal wind vector, c_p the heat capacity of the air at constant pressure, and ρ_{eff} the effective cold air density which is generally equal to the mean air density in the cold air layer ρ_0, except for land use classes describing built-up areas. In urban or industrial canopies the buildings cause displacement of cold air volume and the effective cold air density is calculated by $\rho_{eff} = (1 - b_u)\,\rho_0$ within the canopy and by $\rho_{eff} = \rho_0$ for cold air above it. The fraction of surface covered by buildings b_u and the mean building height h_u are given in Table 1. The displacement effect is based on the assumption that cold air forming outdoor stays outdoor (all windows, doors, etc. are shut).

Id	**class**	z_0 [m]	b_u	h_u [m]	***WAI***	b_v	h_v [m]	***LAI***	***a***	***P*** [W/m^2]
1	Urban (dense)*	0.1	0.6	15.0	3.0	0.0	0.0	0.0	0.0	0.0
2	Residential*	0.1	0.4	8.0	4.0	0.0	0.0	0.0	0.28	8.4
3	Forest*	0.4	0.0	0.0	0.0	0.9	20.0	6.0	0.56	16.8
4	Semi-sealed	0.02	0.0	0.0	0.0	0.0	0.0	0.0	0.64	19.2
5	Industrial*	0.08	0.6	12.0	0.9	0.0	0.0	0.0	0.0	0.0
6	Park*	0.1	0.0	0.0	0.0	0.2	20.0	6.0	1.0	30.0
7	Open space	0.05	0.0	0.0	0.0	0.0	0.0	0.0	1.0	30.0
8	Sealed	0.01	0.0	0.0	0.0	0.0	0.0	0.0	0.28	8.4
9	Water	0.001	0.0	0.0	0.0	0.0	0.0	0.0	0.0	0.0

* land use class with volume friction parameterisation (see Appendix A).

Table 1. Standard settings for some predefined land use classes in KLAM_21. The listed physical parameters are: the aerodynamic roughness length z_0, the surface area fraction covered by buildings b_u, the average building height h_u, the wall area index WAI, the surface area fraction covered by trees b_v, the average tree height h_v, the leaf area index LAI, and the fraction of the maximum local heat loss rate a. The local heat loss rate $P = a \cdot P_{max}$ is listed for $P_{max} = 30$ W/m^2.

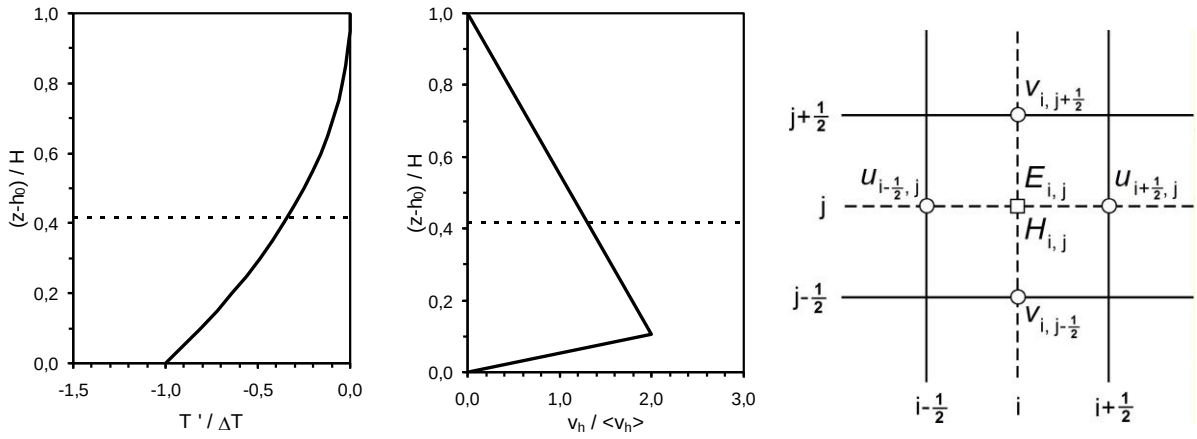

Figure 1. Schematic representations of KLAM_21 model characteristics. Left and centre: Universal vertical profiles of normalised temperature disturbance T'/ΔT and normalised horizontal wind velocity v_h /<v_h> in the cold air layer. The vertical axes show normalised heights above ground level with the dashed lines indicating $\beta=H_{eff}/H$ =5/12. Right: Plain view of the Arakawa C grid structure for horizontal wind components u and v, the total heat deficit E, and the cold air layer depth H. i and j are grid cell indices in west-east and south-north directions.

The air temperature disturbance T' in the cold air layer is assumed to obey a universal parabolic profile (Figure 1) using the scaling parameters ΔT_0 (=3 K) and H_0 (=10 m):

$$T'(x,y,z) = \underbrace{\Delta T_0 \left(\frac{H(x,y)}{H_0} \right)^{1/2}}_{\Delta T(H)} \underbrace{\left(\frac{h_0(x,y) + H(x,y) - z}{H(x,y)} \right)^2}_{f(H,z)} \quad \text{for } h_0 \le z \le h_0 + H \qquad (2)$$

Note that *T'* becomes zero at the absolute height $z=h_0+H$ of the cold air layer top. With the total heat deficit *E* obtained from equation 1, *H* is calculated diagnostically every model time step from the general relation:

$$E = c_p \, H \left\langle \rho_{eff} \, T' \right\rangle \qquad (3)$$

With *T'* defined by equation 2, the total cold air layer depth is given by:

$$H(x,y) = H_0 \left(\frac{E(x,y)}{r_v c_p \langle f \rangle H_0 \Delta T_0} \right)^{2/3} \quad \text{where } \langle f \rangle \text{ is obtained as } \langle f \rangle = 1/3 \qquad (4)$$

The volume reduction factor r_v describes an increased cold air layer depth in urban or industrial canopies due to the displacement of cold air volume by the buildings. For its calculation see Sievers (2005). Observations indicate that only the lower part of the stably stratified cold air layer of depth $H_{eff}=\beta H$ contributes effectively to the forcing of drainage winds, while weak return circulations or regional winds usually dominate aloft between H_{eff} and *H*, where horizontal temperature gradients are less pronounced. In the concept of KLAM_21 the

gravitational forcing acting on a cold air layer is driven by the inclination of its effective height $h_0+H_{eff} = h_0+\beta H$ (see Section 2.2). This follows from energy balance arguments between neighbouring columns of the cold air layer. The value of the factor β depends on the assumed profile of the temperature disturbance T'. Using equation 2 one obtains β=5/12.

2.2 Momentum budget of the cold air layer

The prediction of the velocity and direction of the cold air drainage is based on vertically averaged momentum tendency equations for the two horizontal wind components. In vector form they can be summarised as:

$$\underbrace{\frac{\partial\langle\vec{v}_h\rangle}{\partial t}}_{I} = \underbrace{-\frac{g\,\Delta T\,\langle f\rangle}{T_0}\mathbf{T}^2\cdot\nabla_h\left(h_0+\beta H\right)}_{II} + \underbrace{\overbrace{l\left|\langle\vec{v}_t\rangle\right|\mathbf{D}\cdot\langle\vec{v}_h\rangle}^{a} - \overbrace{\frac{1}{H}c_*\langle\vec{v}_h\rangle\left|\langle\vec{v}_t\rangle\right|}^{b}}_{III} + \underbrace{REG}_{IV}\ , \quad (5)$$

with the wind vector tangential to the surface $\langle\vec{v}_t\rangle = \mathbf{T}^{-1}\cdot\langle\vec{v}_h\rangle$. Local temporal changes in the horizontal wind vector $\langle\vec{v}_h\rangle$ (term *I*) result from imbalances between effective gravitational forcing (term *II*), friction (term *III*), and the effects of a regional wind (term *IV*, see Appendix B). The friction term consists of surface and canopy friction (term *IIIb*, see Appendix A) and the effects of horizontal diffusion (term *IIIa*). T_0 represents a typical mean temperature in the cold air layer and c_* is the friction coefficient which depends on surface roughness length z_0 and on H_{eff}. In forested and urban areas c_* is also a function of canopy height and density (see Appendix A). The mixing length l for horizontal diffusion of momentum is set to the typical nocturnal value l=1 m. The projection operator **T** from the tangential to the horizontal plane and the differential operator **D** are:

$$\mathbf{T} = \begin{pmatrix} 1/\sqrt{1+\left(\frac{\partial h_0}{\partial x}\right)^2} & 0 \\ 0 & 1/\sqrt{1+\left(\frac{\partial h_0}{\partial y}\right)^2} \end{pmatrix} \quad \text{and} \quad \mathbf{D} = \begin{pmatrix} \frac{\partial}{\partial y^2} & 0 \\ 0 & \frac{1}{\partial x^2} \end{pmatrix} \quad (6)$$

The effective gravitational forcing (term *II* in Eq. 4) is proportional to the inclination of the effective cold air layer height relative to sea level $\nabla_h\left(h_0+\beta H\right)$ and the maximum temperature disturbance at the surface $\Delta T = T'(x, y, z=h_0)$.

For some applications, such as model comparison with surface station observations (see Section 5.2), KLAM_21 approximates the vertical drainage wind profile $v_h(z)$ by a universal triangular wind profile with a wind speed maximum $\vec{v}_{h,\,\max} = 2\langle\vec{v}_h\rangle$ at the height $0.25H_{eff}$. Wind speed decays linearly from this value to zero wind at the surface and at H (Figure 1). Comparison with published profiles of

observed drainage winds (Whiteman, 2000) shows that the universal wind profile $v_h(z)$ used by KLAM_21 mainly resembles the shape of thermally driven down-slope winds, while thermally driven down-valley winds in several valleys show a wind speed maximum at significantly great heights above ground, i.e. at up to about half height of the surface temperature inversion.

3. Model numerics, initialisation and boundary conditions

Integration over time is carried out on a regular (orthogonal) Arakawa C grid (Figure 1) using dynamically calculated time steps. Spatial gradients are determined as centred differential quotients and advection is calculated using an upstream donor cell algorithm. At the model domain boundaries inflow of cold air is zero, while outflow of cold air is slightly reduced by an empirical function to avoid unrealistic model results when modelling the entire drainage domain is not feasible.

The model KLAM_21 is initialised with neutral stratification and zero wind. Model simulations start in the evening with the onset of surface cooling (around sunset).

The standard size of the computational domains can reach up to 3000 x 3000 grid cells. Grid resolutions usually range between 10 m and 500 m. High resolution simulation can be limited to one or more nested inner grid domains, while the coarser outer domain is covering the entire airshed of interest.

4. Model input and output data

The model requires orthogonal, equidistant raster ASCII data of terrain height and land use. Table 1 shows a selection of pre-defined land use classes together with their assigned physical parameters. Overall, around 20 pre-defined land use classes are currently available. Users have the possibility to change physical parameters of these classes and are able to define new land use classes.

Model output is provided as ASCII raster data for the entire domain at selected output times (e.g. at certain hours) and as continuous ASCII time series of individual model grid cells or spatially averaged values over rectangular subdomains with user selectable time intervals (e.g. 10-minutes intervals). The main model output parameters are:

- the (vertically integrated) heat deficit in the cold air layer $E(x,y)$,
- the effective cold air layer depth $H_{eff}(x,y)$,
- vertically averaged horizontal wind components $u(x,y)$ and $v(x,y)$,
- the horizontal wind components at a selectable height z above ground $u_z(x,y)$, $v_z(x,y)$, and
- (optionally) mean tracer concentration in the cold air layer $c(x,y)$.

The horizontal wind components at a selectable height above ground $u_z(x,y)$ and $v_z(x,y)$ are only rough estimates based on vertically averaged horizontal wind components and the assumption of the universal triangular wind profile shown in Figure 1.

5. Comparison with observations

Since KLAM_21 is a single-layer model, the most suitable observations for the evaluation of simulations are vertical profiles of wind and air temperature covering a height range from the surface to at least the top of the surface based stable layer (cold air layer).

Sequences of observed temperature profiles can be used to evaluate the

vertically integrated heat deficit in the cold air layer and its temporal changes from KLAM_21 simulations. This works particularly well when a vertical temperature profile is measured around sunset, .i.e. at the start time of a model simulation. Furthermore, observed temperature profiles can be used to evaluate the simulated total cold air layer depth (see section 5.1).

For the evaluation of the simulated wind field the observed wind profile data averaged over the depth of the surface based cold air layer can be compared to the simulated layer averaged wind vector. Modern remote sensing instruments such as wind LIDARs can provide the possibility to evaluate simulated cross-sectional volume fluxes of drainage flows along slopes or valleys (Clements et al., 1989; Banta et al., 1997). If observed wind data are only available from surface stations (at a single height above ground level), the selectable height above ground for additional KLAM_21 wind output is set to anemometer height to enable a less sophisticated comparison with simulated wind fields (see section 5.2). Photographs or videos of smoke experiments provide an additional option to qualitatively evaluate simulated wind fields and tracer dispersion (Sievers, 2005).

The local heat loss rate P represents the sum of turbulent and radiative cooling in the cold air layer. To evaluate P, observed divergences of the turbulent sensible heat flux and the net longwave radiation flux integrated vertically over the depth of the cold air layer would be particularly suitable (Sun et al., 2003; Nakamura and Mahrt, 2006). Unfortunately, such observations are rarely available. But observations of the net longwave radiation balance at the surface during nighttime are much more common and represent a first approximation for the upper limit of the magnitude of P, for cases with negligible latent heat and ground heat fluxes. All simulations presented in Sections 5.1 to 5.3 are carried out with land use dependent P values given in Table 1 ($P=a \cdot P_{max}$, P_{max} = 30 W/m^2). Idealised simulations based on these settings by Sievers (2005) show that resulting growth rates of the cold air layer depth H compare well with volumetrically derived values from observational studies in Germany (VDI, 2003).

Sections 5.1 to 5.3 provide comparisons of the cold air layer depth, the near surface wind speed and direction, and the spatial drainage wind pattern simulated by KLAM_21 with available observations.

5.1 Cold air layer depth

During a multi-day fair weather episode in summer 2004 radiosondes were released from the floor of a valley in central Germany to capture vertical temperature profiles shortly after sunrise. The location of the study site is depicted in Figure 2 and in the right panel of Figure 3. The surroundings of the release site at about 200 m above sea level (asl) are open spaces, while nearby hill tops are partly covered by forest and reach up to about 450 m asl.

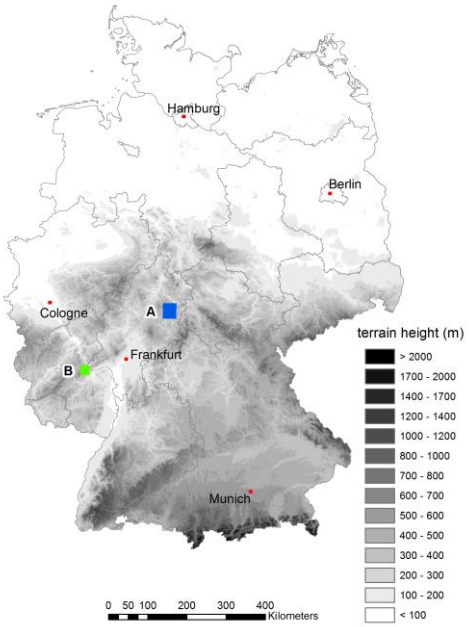

Figure 2. Topographic map of Germany with KLAM_21 model domains for case studies discussed in Section 5.1 (domain A) and Section 5.2 (domain B). © GeoBasis-DE / BKG 2016.

The left panel of Figure 3 shows measured vertical temperature profiles up to 1000 m above ground level (agl) from three consecutive mornings. The temperature values have been normalised by the maximum temperature T_{max} observed at the top of the temperature inversion. A fog layer developed in the morning of 28 July at about 04:30 Central European Summer Time (CEST). At the time of the radiosonde release at 07:16 CEST the fog layer had a thickness of about 170 m. The almost adiabatic stratification in the fog layer is associated with top-down mixing caused by the nocturnal cooling process at the top of the fog layer.

Above the temperature inversion all three soundings show almost dry adiabatic stratification which is typical for nocturnal residual layers under fair weather conditions. Maximum near surface temperatures observed in the afternoons of the previous day coincide very well with temperatures determined by dry adiabatic extrapolation from T_{max} at the inversion top down to the surface. This strongly indicates that the nocturnal heat loss documented by the temperature profiles had been caused mainly by local heat loss due to radiative and turbulent cooling and by terrain induced drainage winds, while other processes such as large scale advection were of negligible magnitude.

For comparison with observations a KLAM_21 simulation with 100 m resolution was carried out for a model domain of 21 x 24 km^2 (domain A in Figure 2), covering all cold air sources relevant for the radiosonde release site. Within a 7 x 6 km^2 subdomain nested around the release site (shown in the right panel of Figure 3) the simulation was performed with a higher resolution of 20 m. The onset of surface cooling occurred at around 20:00 CEST, which therefore represents the start time of the model simulation.

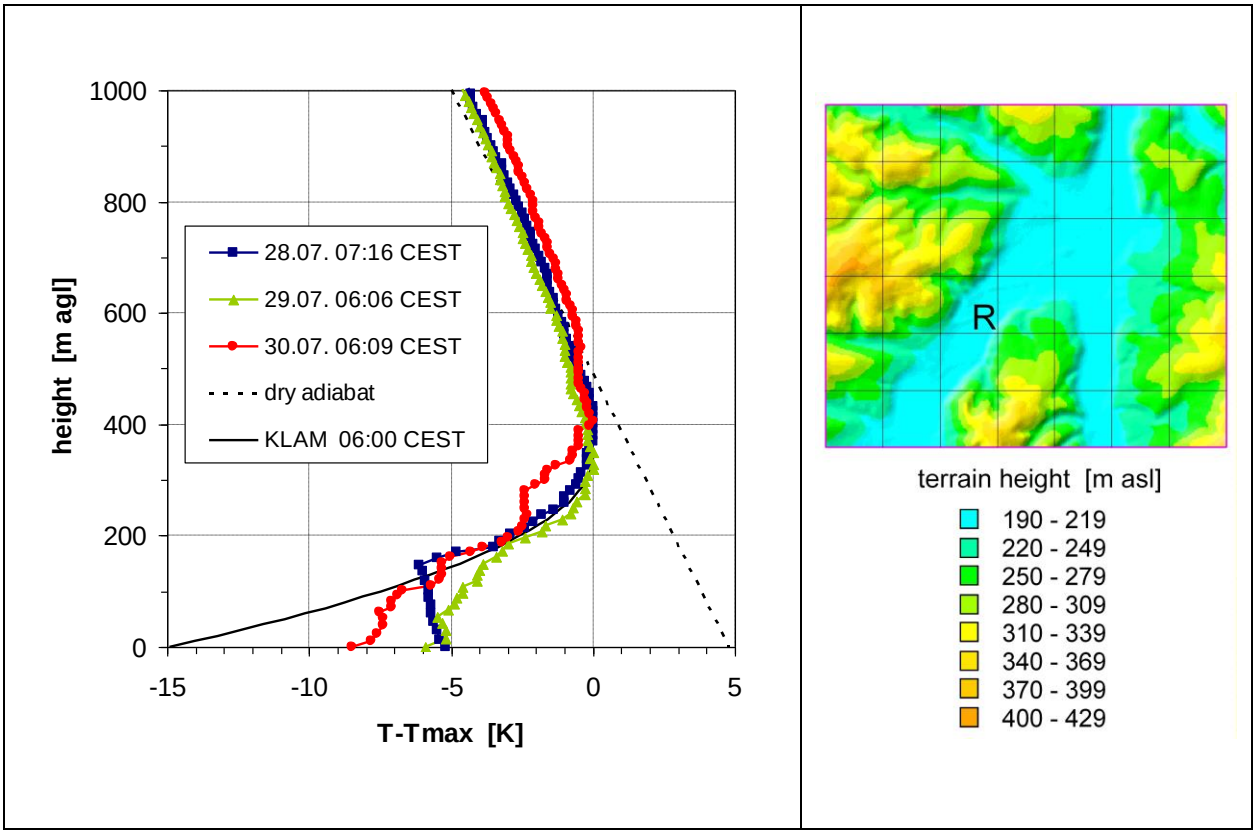

Figure 3. Normalised vertical profiles of air temperature observed by radiosondes on three consecutive summer mornings (28 - 30 July) shortly after sunrise. The location of the radiosonde launch site (R) in the center of a valley is indicated in the map on the right hand side, showing the 7 x 6 km^2 high-resolution model subdomain. The vertical profiles are normalised by the maximum air temperature at the top of the temperature inversion. An approximately 170 m deep fog layer developed in the morning of 28 July. The corresponding KLAM_21 profile represents a spatial average over 3 x 3 grid cells after 10 hours of simulation.

Averaged over 3 x 3 grid model cells around the release site, a total cold layer depth H of 381 m was simulated after 10 hours simulation time (at 06:00 CEST). The corresponding normalised universal temperature disturbance profile of KLAM_21 (Eq. 2) has been added to the neutrally stratified basic state stratification (assuming $T(H)$-T_{max} = 0) and is shown in Figure 3 together with the observed profiles. The observed total cold air layer depth H is given by the height of T_{max} at the inversion top. The observed values of H are 401 m (28 July), 334 m (29 July), and 407 m (30 July). The maximum relative difference between simulated and observed values of H is less than 15% which can be considered a good agreement.

5.2 Wind speed and direction

Observations of wind speed and direction at 10 m agl (above ground level) were made at two surface stations in hilly terrain in western Germany in September and October 2003. Station 1 was located at 300 m asl (above sea level)in a west to east oriented tributary valley, while station 2 was set up in the northwest to southeast

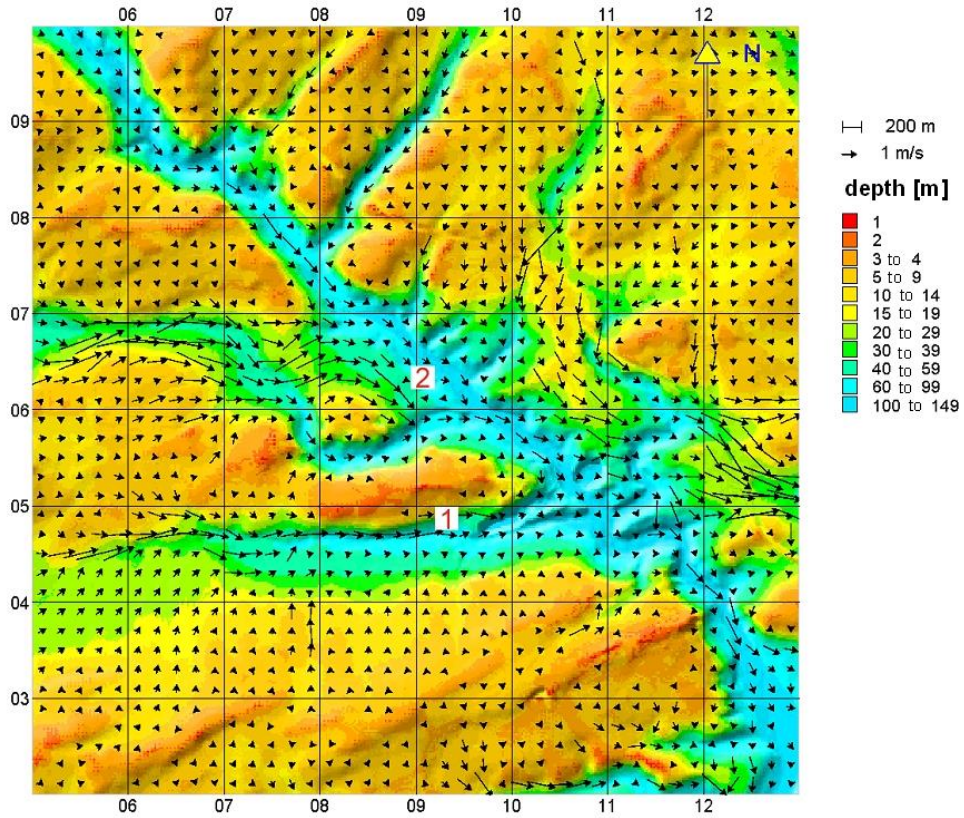

Figure 4. KLAM_21 results of effective cold air layer depth (colour code) and wind at 10 m agl (vectors) after a simulation time of 5 hours (23:00 CET). For reasons of clarity only every tenth wind vector is shown. No wind vectors are shown if wind speed is below 0.05 m/s. Axis labels show distance from the south-western corner of the model domain in km. Terrain height structures are indicated by shading of the colour code. Numbers 1 and 2 indicate the locations of surface stations used for model evaluation.

oriented main valley at 290 m asl (Figure 4). Both stations were located slightly above the valley floor where agriculture is the dominating land use. The hilltops around the valleys are mostly covered by forest and reach up to 450-600 m asl.

Figure 5 shows the time series of air temperature, wind velocity, and direction recorded at the two surface stations during a 7 day fair weather period (15-21 September). The observed temperature variations show undisturbed diurnal cycles with an amplitude between 15 and 20 K.

The wind observations document well pronounced up-valley winds during daytime and down-valley winds during nighttime. Cross-valley winds occurred only occasionally, mainly during the wind transition periods between the up-valley and down-valley wind regimes. While wind velocity at the two stations was of similar magnitude during daytime, the intensity of nocturnal down-valley winds at station 1 was clearly stronger than at station 2.

Hourly wind data averaged over all 17 fair weather days during the measurement period are shown in Figure 6. Drainage winds are evident for the period between 19:00 and 08:00 Central European Time (CET) with wind velocities and direction being almost constant throughout the night

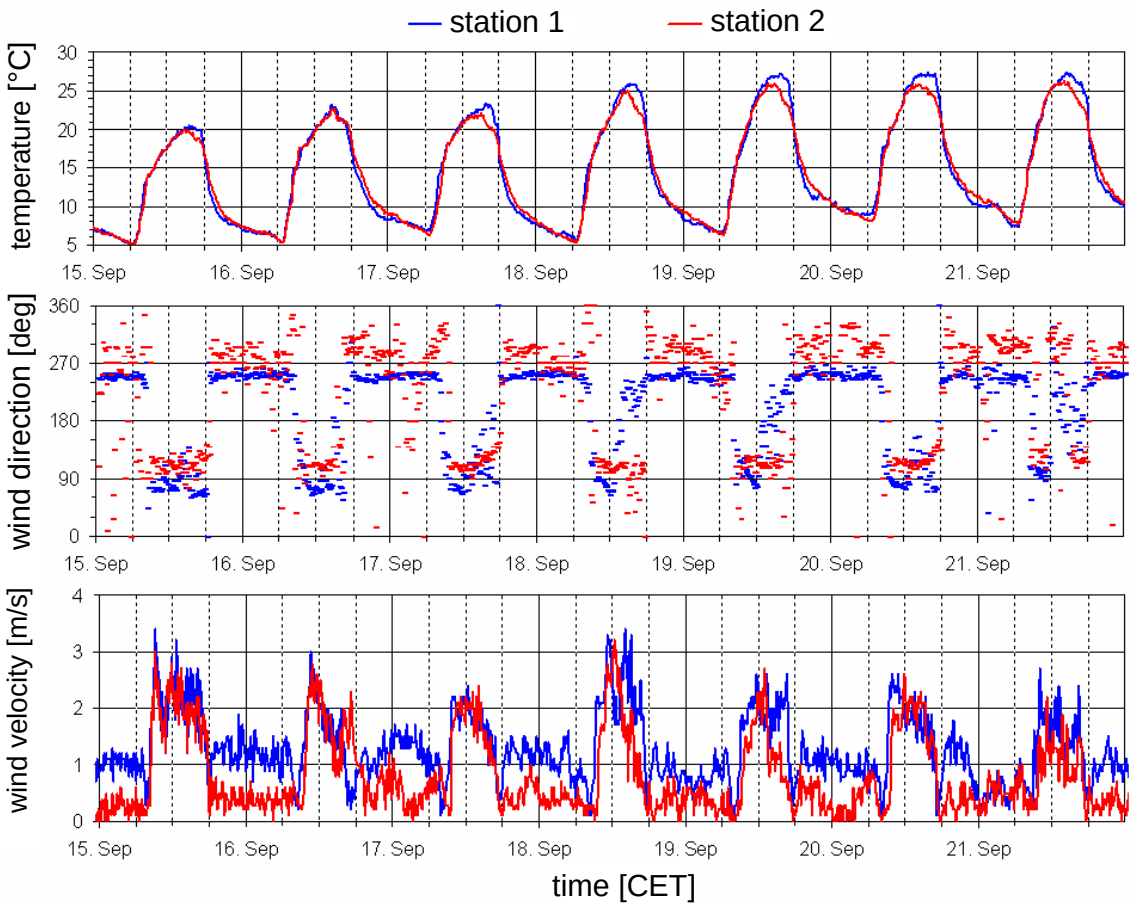

Figure 5. 10-minute average time series of air temperature at 2 m agl and of wind velocity and wind direction at 10 m agl observed at two stations during the fair weather period 15-21 September 2003. The locations of station 1 and 2 are shown in Figure 4.

at both stations. The magnitudes of the observed mean drainage wind velocities were about 1.0 m/s at station 1 and about 0.4 m/s at station 2.

For comparison with observations, a KLAM_21 simulation with 100 m resolution was carried out for a model domain of 14 x 15 km^2 (domain B in Figure 2), covering all relevant cold air sources for the two measurement sites. For the nested sub-domain of 8 x 8 km^2 shown in Figure 4 a higher spatial resolution of 20 m was chosen for the simulation. The observed onset of surface cooling occurred at about 18:00 CET, which represents the start time of the model simulation. Figure 4 depicts the simulated effective cold air layer depth and the horizontal wind vectors after 5 hours of simulation (23:00 CET). The simulated down-slope and down-valley winds caused accumulation of cold air in the valleys and resulted in an effective cold air layer depth of about 100 m at the two stations. About 1.3 km west-northwest of station 2 the down-valley winds in a tributary valley take a short-cut exit over a saddle with elevations lower than the cold air layer top.

Overall, the simulated hourly wind velocity and direction for the two station sites agree quite well with the wind observations averaged over all fair weather days (Figure 6). Only at the beginning of the night at station 2 stronger differences

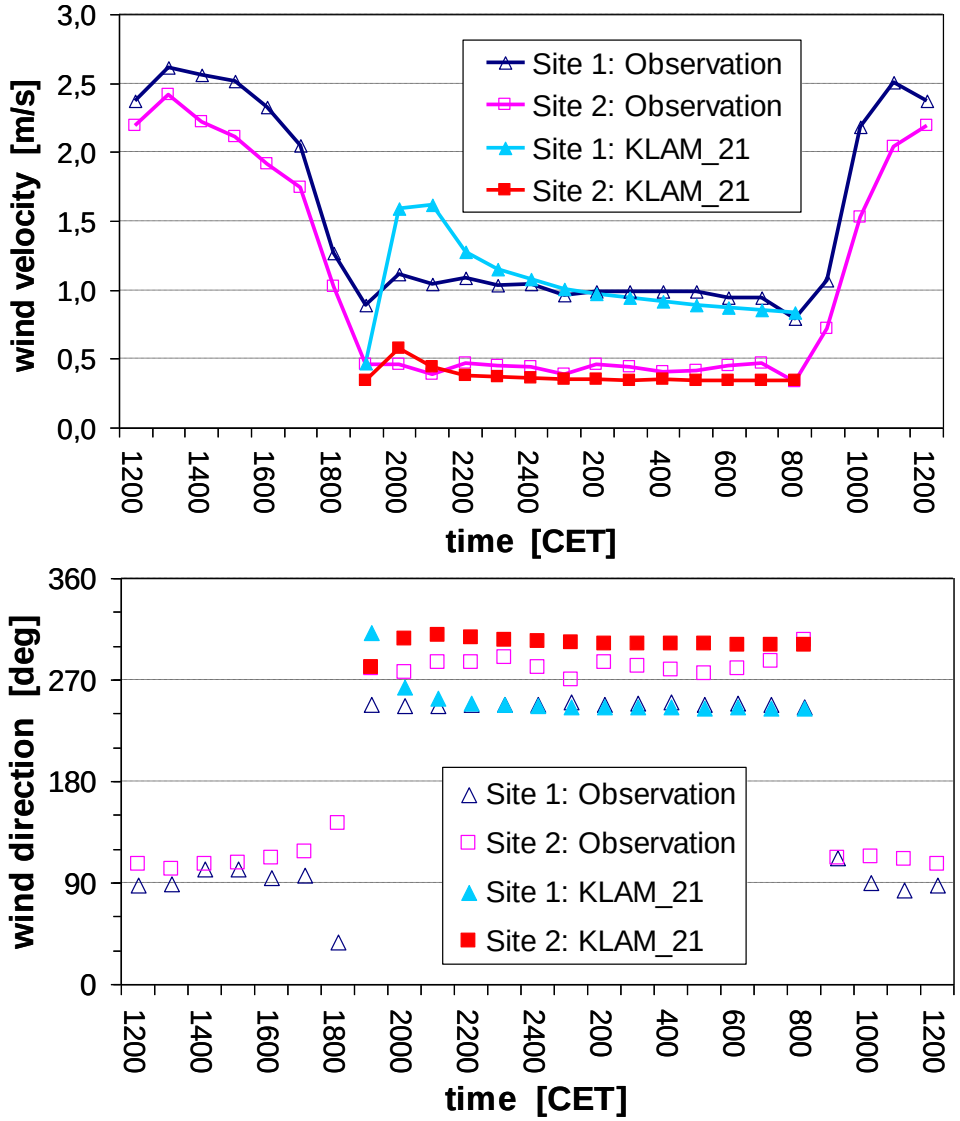

Figure 6. Comparison of observed and simulated hourly wind velocity (top) and direction (bottom) data at 10 m agl for two surface station sites. The locations of station 1 and 2 are shown in Figure 4. The observed wind data have been temporally averaged over 17 fair weather days in autumn 2003. The simulated wind data have been spatially averaged over 3 by 3 model grid cells centred at the station locations.

are noticeable by a 50% underestimation in wind speed at 19:00 CET, followed by a 50% overestimation at 20:00 and 21:00 CET. Simulated wind direction at station 2 is mostly from west-northwest while observations show a more westerly flow direction. A model underestimation of the mentioned airflow over the saddle to the west of station 2 most likely explains the difference between modelled and observed wind direction. For the nocturnal hours between 19:00 and 08:00 CET the mean absolute errors (Willmott and Matsuura, 2005) for the simulated wind speed are 0.16 m/s at station 1 and 0.08 m/s at station 2, while mean absolute errors for simulated wind direction are 8.0 deg at station 1 and 19.5 deg at station 2.

5.3 Spatial drainage wind pattern

Nocturnal flow patterns during high pressure weather situations can be quite complex when orographically induced drainage winds interact with landuse induced thermal wind systems and/or when scale interaction between multiple thermal wind systems is important. Both are clearly the case in Christchurch (New Zealand), where local drainage winds from the Port Hills and regional scale drainage winds from the Southern Alps interact with coastal land breezes and country breezes initiated by Christchurch's urban heat island (Ryan, 1975; McKendry et al. 1986; Kossmann and Sturman, 2004; Spronken-Smith et al., 2006).

The 24h health guide line for PM_{10} is frequently exceeded in Christchurch during wintertime. Highest hourly concentration values typically occur between sunset and midnight, when emissions from domestic heating are highest and dispersion is strongly limited by local winds and surface temperature inversions (Spronken-Smith et al., 2002; Corsmeier et al., 2006). To test the flow simulation capabilities of KLAM_21 in such terrain settings, the nocturnal surface wind patterns observed over Christchurch during a case study of the CAPS2000 field campaign (Kossmann and Sturman 2004) are compared to results from a model simulation.

Figure 7 shows observed surface winds in the Christchurch area about 3 h after sunset on 8 June 2000, which was a clear winter night with weak ambient winds and an observed 24h mean PM_{10} concentration of 83 μg m^{-3}. At a regional scale, the surface wind field is characterised by drainage winds down the Canterbury Plains and land breezes along the coastline. Flow splitting of the drainage winds is caused by the terrain elevations of the Port Hills and Banks Peninsula (see left panel of Figure 7). Over the urban area of Christchurch northwesterly regional drainage winds down the Canterbury Plains converge with local southerly drainage winds from the Port Hills (see right panel of Figure 7). This zone of flow convergence is characterised by very weak winds that favour the accumulation of air pollutants. Later in the night the regional scale northwesterly drainage winds become more dominant and the convergence zone is shifted southward towards the Port Hills (Corsmeier et al., 2006).

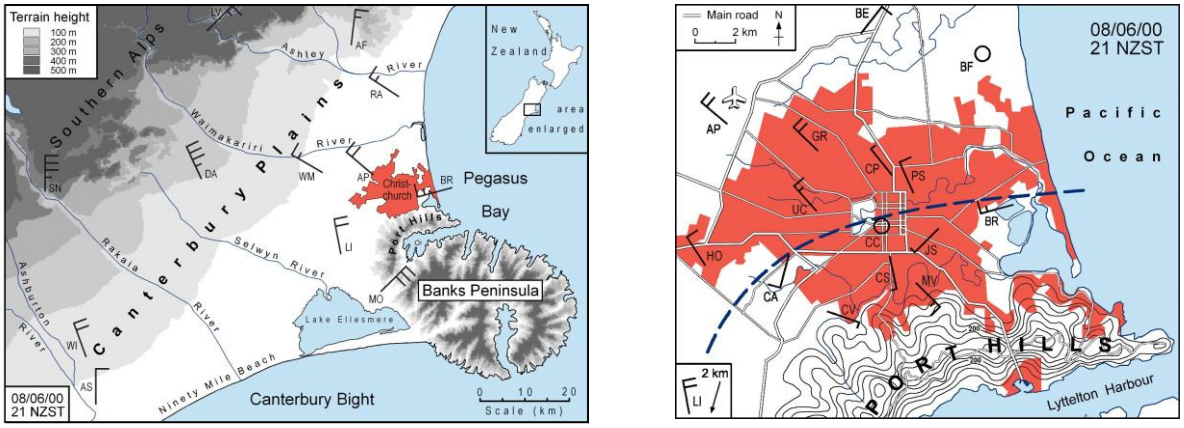

Figure 7. Topography of study area on the South Island of New Zealand and observed surface winds on 8 June 2000, 21:00 NZST. Long barbs indicate 1 m s^{-1} each, short barbs indicate 0.5 m s^{-1}, and open circles indicate calms. Left: Coastal Canterbury area. Right: Christchurch urban area. The dashed line illustrates the convergence zone of regional and local drainage winds.

Selecting a 150 x 140 km^2 KLAM_21 model domain ensured large parts of coastal Canterbury are captured (Figure 8). The city of Christchurch and most parts of the Port Hills are located within the nested (inner) domain of 40 x 35 km^2. The simulation was carried out with a spatial resolution of 100 m in the inner domain and 500 m in the outer domain. Sunset is assumed to be at 18:00 NZST (typical for midwinter). Terrain height and land use data represent conditions during the year 2000 (prior to the Darfield and Christchurch earthquakes in 2010 and 2011, respectively).

Figure 8 shows KLAM_21 results of the regional surface wind field after 3 hours of simulation (21:00 NZST). The structure and intensity of the main observed flow features, such as cold air drainage down the Canterbury Plains, land breezes along the coastlines, and flow splitting northwest of Banks Peninsula are well captured by the model. Over the city of Christchurch the model also simulates the observed convergence of regional drainage winds down the Canterbury Plains and local drainage winds from the Port Hills, and the associated poor ventilation (low cold air volume fluxes) over the Christchurch urban area (Figure 9). The minimum in the modelled effective cold air layer depth over the city centre and the eastern suburbs results from the low or zero heat loss rate *P* for residential or dense urban land use in the city (see Table 1) and causes the formation of country breezes, which are superimposed on the drainage winds and land breezes (Figure 9).

Visualisation of wind data from high resolution simulations for large domains in complex terrain can be difficult because it is often not possible to draw wind vectors for every model grid cell (see Figures 8 and 9). For the Christchurch case study it proved helpful to calculate and illustrate streamlines to enable an understanding of the simulated interaction of multiple thermal wind systems. For example, the streamlines calculated at 21:00 NZST (Figure 10) clearly reveal that airflow over the southeastern suburbs originates from cold air formation and drainage in the valleys on the northern side of the Port Hills, while the other parts of the city are already exposed to the larger scale drainage winds down the Canterbury Plains.

6. Discussion and conclusion

KLAM_21 is a single layer model designed to simulate vertically averaged drainage winds that develop in stably stratified nocturnal boundary layers over complex terrain. The simulation of the speed, direction, and depth of drainage winds is computationally inexpensive and can be performed for large domains with a very high spatial resolution. The presented comparisons of KLAM_21 simulations with observations indicate that the quality of simulated cold air layer depth and near surface drainage wind speed and direction is acceptable for many practical applications. Besides the relief generated drainage winds, KLAM_21 has also shown its capability to simulate the effects of other superimposed nocturnal thermally driven wind systems, such as country-breezes and land-breezes. Good agreement between KLAM_21 simulation results and observations has also been found by other model users (Schwab and Zachenbacher, 2009; Sachsen et al. 2013). Model users are encouraged to conduct additional and more detailed model evaluations, e.g. using observational data from more comprehensive field campaigns such as CASES-99 (Poulos et al., 2002), T-REX (Grubisic et al., 2008), or COLPEX (Price et al., 2011).

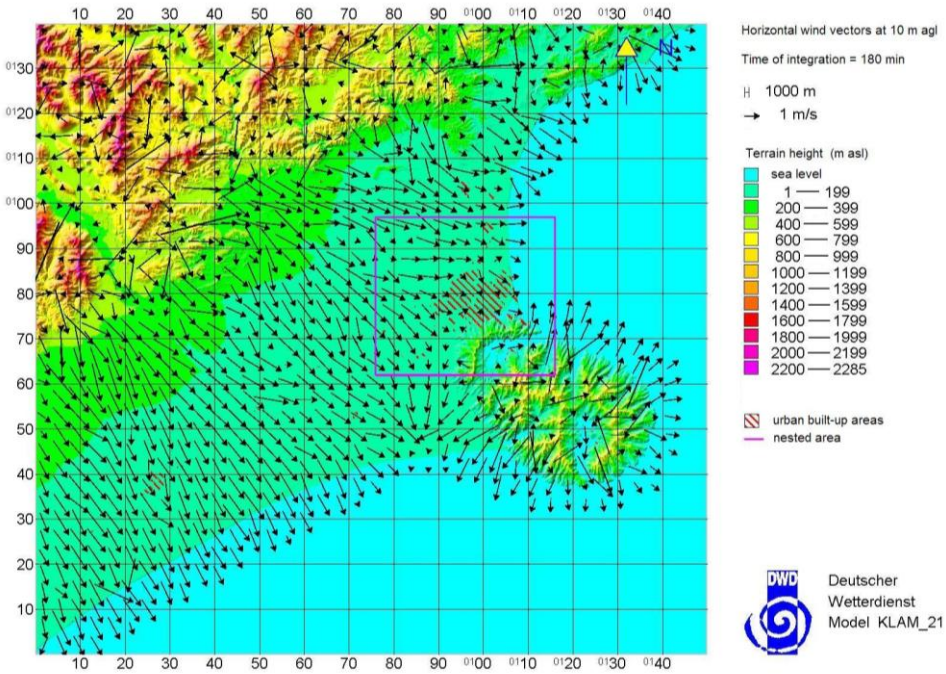

Figure 8. Computational domain of the KLAM_21 simulations for the area of Christchurch, New Zealand. The nested area (40 km x 35 km) with higher spatial resolution is indicated by the rectangle around the area of Christchurch. Colour shading indicates terrain height above sea level. Arrows represent horizontal wind vectors at 10 m above ground level after 3 h of simulation (21:00 NZST). Wind vectors are only plotted at 4 km intervals for wind speeds exceeding 0.05 m s^{-1} and for H > 10 m.

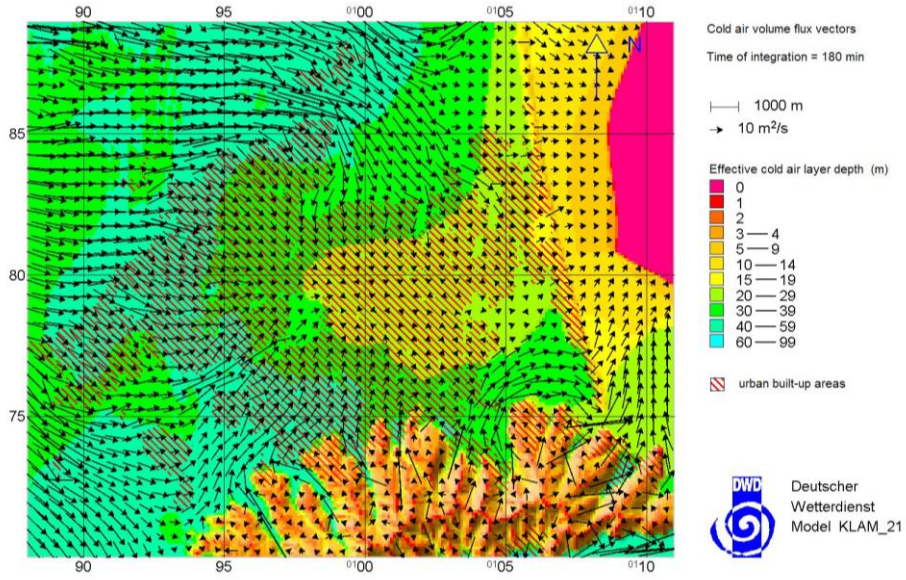

Figure 9: Vectors of the vertically integrated cold air flux (volume flux) density and effective cold air layer depth H_{eff} over the Christchurch area after 3 h of simulation (21:00 NZST). The shape of the terrain elevation is indicated by sun shading superimposed on the colour shading of the effective cold air layer depth. Volume flux vectors are only plotted at 500 m intervals. Urban built-up areas are marked by red diagonal stripes.

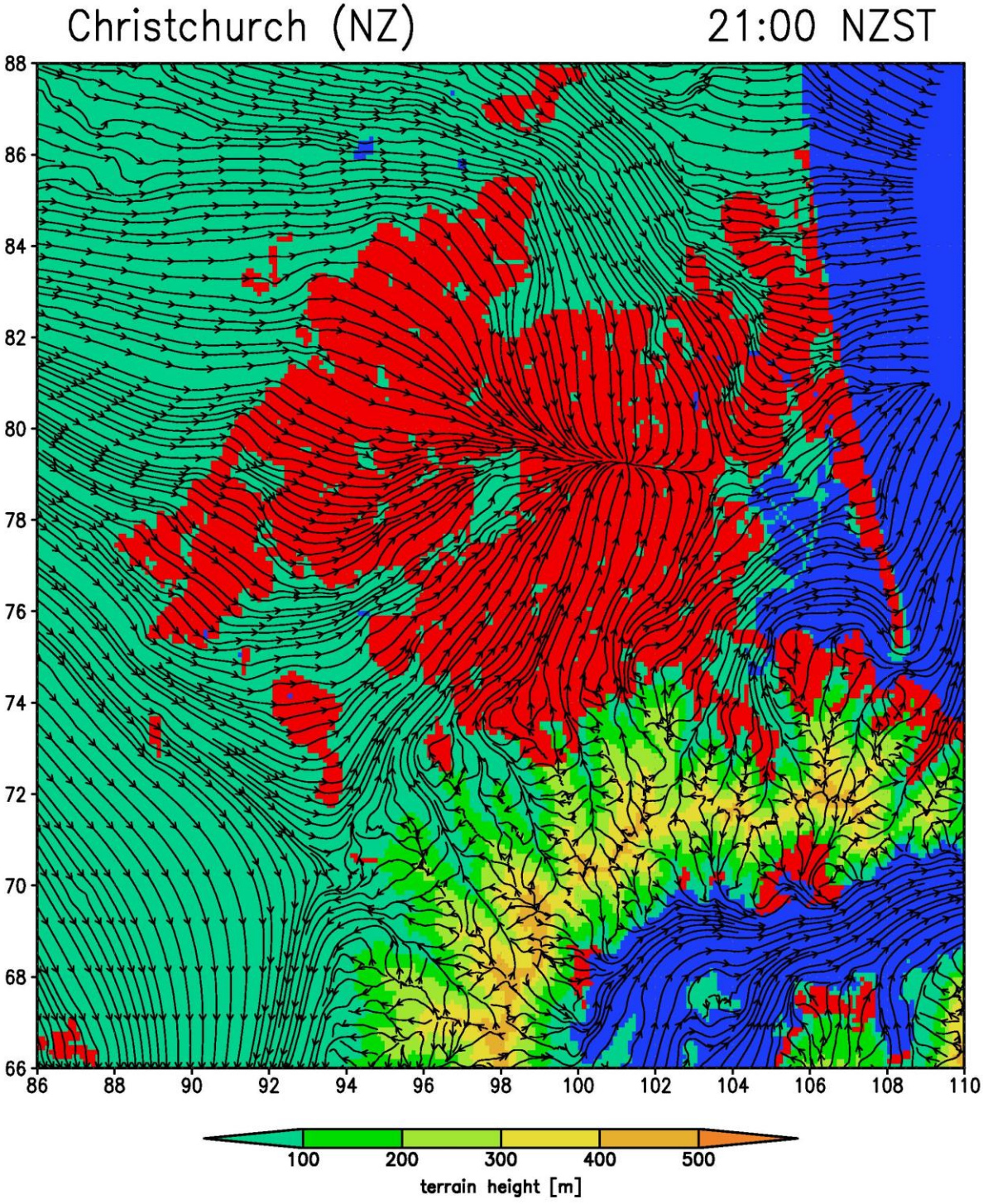

Figure 10. Modelled streamlines of cold air drainage over Christchurch 3 h after sunset (21:00 NZST). Red and blue indicate urban areas and water surfaces, respectively. Axis labels show distance from the south-western corner of the model domain in km.

It should be noted that the simplifications of the model physics, which are the main reason for the computational efficiency of the model, also cause some limitations regarding possible model applications. For example, the effects of internal gravity waves or vertically varying wind directions within the cold air layer can not be simulated. The model is also less suitable when local advection of momentum plays a very important role, or for situations with a stably stratified ambient atmosphere (KLAM_21 assumes a neutrally stratified atmosphere above the developing cold air layer).

The prescribed local heat loss rates P for each land use type makes the model primarily suitable for the simulation of drainage winds under idealised fair weather conditions. This approach of using prescribed values of P has the significant advantage that no model schemes for thermal surface energy exchange, atmospheric radiation or boundary layer turbulence are needed. The latter means that all problems of turbulence parameterisations under intermittent turbulence conditions or under very stable stratification (Mahrt, 1998; Sun et al., 2002; Acevedo and Fitzjarrald, 2003; Salmond and McKendry, 2005) are circumnavigated with minimal restrictions on the quality of simulated wind fields but with strong benefits for the computational duration of model simulations.

Over the years the model has proven to be a valuable tool for consultancy in urban planning and landscape planning, with most applications of KLAM_21 focussing on aspects of air quality (e.g. urban ventilation) or frost protection (cold air ponding). In New Zealand KLAM_21 could be used to study frost problems in the fruit and wine growing industries and to investigate possible effects of drainage winds on the ventilation or accumulation of air pollutants in complex terrain settings. Besides the presented simulations with grid spacing between 20 m and 500 m (Section 5), the model has proven to work successfully at a spatial resolution of 2 m (Sachsen et al., 2013) to study particularly small scale modifications in terrain or land use. Furthermore, the simplicity of the model and the graphical user interface provides an interesting modelling capability for users without high-level expertise in atmospheric modelling (e.g. regional government agencies or scientists specialised in observational studies).

Future work could include comparisons between model results from KLAM_21 and from 3-dimensional mesoscale models or LES models. Preferably this should be done for idealised cases, e.g. sensitivity studies to determine nocturnal pooling/draining indices for valleys of varying shape and size (Kossmann, 2015). Such a comparison would raise the awareness of the advantages and limitations of 2-dimensional (single-layer) models versus 3-dimensional models. Further developments of KLAM_21 could address improved universal profiles of $T'(z)$ and $v_h(z)$ (see Figure 1), terrain effects on sunset time to consider spatially varying onset times of surface cooling (Schwab and Zachenbacher, 2009), or options to use time dependent local heat loss rates P and ambient (regional) winds to make the model more suitable for comparison with observations.

Appendices A to C provide additional details about parameterisations of surface and canopy friction, the treatment of ambient (regional) winds, and the simulation of the dispersion of an inert tracer. A published report by Sievers (2005) provides a full description of KLAM_21 with additional model features, such as the possibility to simulate flow over and around wall like obstacles (e.g. sound protection walls along highways and railways near settlements).

Acknowledgements

The authors thank their colleagues for their contributions to the development, improvement, and evaluation of the cold air drainage model KLAM_21. We also thank Heidelore Turau for providing Figure 2.

Simulations for comparison with observations have been performed with KLAM_21 model version 1.125 (Sievers, 2005). The graphical user interface of the current model version 2.012 offers additional options for visualising place names, borderlines or urban/rural boundaries in the model domain.

The authors thank the reviewers for helpful comments to improve the manuscript. Support of the CAPS2000 field campaign by the New Zealand Public Good Science Fund under contract no. C01X0011 'Urban Air Quality Processes' and the provision of observational data by the University of Canterbury, the National Institute for Water and Atmospheric Research, Environment Canterbury, the National Rural Fire Authority, the Selwyn Plantation Board and the Christchurch City Council are gratefully acknowledged.

References

Acevedo, O.C. and Fitzjarrald, D.R., 2003: In the core of the night – effects of intermittent mixing on a horizontally heterogeneous surface. *Boundary-Layer Meteorology*, **106**, 1-33.

Appelhans, T., Zawar-Reza, P. 2010: A modelling study of particulate matter dispersion under dominant surface wind regime modes in Christchurch, New Zealand. *Air Quality & Climate Change*, **44**(1), 24-28.

Banta, R.M., Shepson, P.D., Bottenheim, J.W., Anlauf, K.G., Wiebe, H.A., Gallant, A., Biesenthal, T., Olivier, L.D., Zhu, C.-J., McKendry, I.G., and Steyn, D.G., 1997: Nocturnal cleansing flows in a tributary valley. *Atmospheric Environment*, **31**, 2147-2162.

Broadbent, A., Cullen, N.J., Zawar-Reza, P., 2010: Wintertime numerical modelling of PM_{10} air pollution in Milton, Otago, New Zealand: Boundary layer structure, effects of data assimilation, and reaching national environmental standards. *Air Quality & Climate Change*, **44**(4), 22-28.

Burns, P. and Chemel, C., 2014: Evolution of cold-air-pooling processes in complex terrain. *Boundary-Layer Meteorology*, **150**, 423-447.

Clements, W.E., Archuleta, J.A., and Hoard, D.E., 1989: Mean structure of the nocturnal drainage flow in a deep valley. *Journal of Applied Meteorology*, **28,** 457-462.

Corsmeier, U., Kossmann, M., Kalthoff, N., and Sturman, A.P., 2006: Temporal evolution of winter smog within a nocturnal boundary layer at Christchurch, New Zealand. *Meteor. Atmos. Phys*., **91**, 129-148.

Fitzharris, B.B., Crooks, J.K., Gazzard, J.M., Geden, B.L., Graham, B.J., Symon, J.E., Weedon, B.G., 1980: Temperature and airflow patterns within the Cromwell Basin under frost conditions. *Geography Discussion Papers, No. 23*, Published by Department of Geography, University of Otago, New Zealand.

Garrett, A.J. and Smith, F.G., 1984: Two-dimensional simulations of drainage winds and diffusion compared to observations. *Journal of Climate and Applied Meteorology*, **23**, 597-610.

Gross, G., 1989: Numerical simulations of nocturnal flow systems in the Freiburg area for different topographies. *Contr. Atmos. Phys.*, **62**, 57-72.

Grubisic V., Doyle, J.D., Kuettner, J., Mobbs, S., Smith, R.B., Whiteman, C.D., Dirks, R., Czyzyk, S., Cohn, S.A., Vosper, S., Weissmann, M., Haimov, S., de Wekker, S.F.J., Pan, L.L., Chow, F.K, 2008: The Terrain-Induced Rotor Experiment - A field campaign overview including observational highlights, *Bulletin of the American Meteorological Society*, **89**, 1513–1533.

Lageron, Y., Staquet, C., and Chemel, C., 2010: Turbulent mixing in a katabatic wind under stable conditions. *Meteorologische Zeitschrift*, **19**, 467-480.

Kossmann, M. and Sturman, A.P., 2004: The surface wind field during winter smog nights in Christchurch and coastal Canterbury, New Zealand. *Int. J. Climatology*, **24,** 93-108.

Kossmann, M., 2015: Simulationen zur Durchlüftung von Tälern während windschwacher Strahlungsnächte, METTOOLS IX, Offenbach am Main, 17-19 March 2015, *Annalen der Meteorologie*, **47**, 111-112.

McGowan, H.A., Sturman, A.P., 1993: Synoptic and local effects on the climate of the Waimate area, South Canterbury. *Weather and Climate*, **13**, 22-33.

McGowan, H.A., Sturman, A.P., 1996: Interacting multi-scale wind systems within an alpine basin, Lake Tekapo, New Zealand. *Meteorology and Atmospheric Physics*, **58,** 165-177.

Mahrt, L., 1998: Stratified atmospheric boundary layers and breakdown of models, *Theoretical and Computational Fluid Dynamics*, **11**, 263–279.

Mattson, J.O. and Nordbeck, S, 1980: Modelling cold air patterns. *Geografiska Annaler*, **62**, 119-129.

McKendry, I.G., Sturman, A.P., Owens, I.F., 1986: A study of interaction of multi-scale wind systems, Canterbury Plains, New Zealand. *Meteorology and Atmospheric Physics*, **35**, 242–252.

Nakamura, R., Mahrt, L., 2006: Vertically integrated sensible-heat budgets for stable nocturnal boundary layers. *Quarterly Journal of the Royal Meteorological Society*, **132,** 383–403.

Polous G.S., Blumen, W., Fritts, D.C., Lundquist, J.K., Sun, J., Burns, S.P., Nappo, C., Banta, R., Newsom, R., Cuxart, J., Terradellas, E., Balsley, B., Jensen, M., 2002: CASES-99: A comprehensive investigation of the stable nocturnal boundary layer. *Bulletin of the American Meteorological Society*, **83**, 555-581.

Powell, S., 2014: The spatial variation of minimum near-surface temperature in complex terrain: Marlborough vineyard region, New Zealand. PhD Thesis, University of Canterbury.

Price J. D., Vosper, S., Brown, A., Ross, A., Clark, P., Davies, F., Horlacher, V., Claxton, B., McGregor, J.R., Hoare, J.S., Jemmett-Smith, B., Sheridan, P., 2011: COLPEX: Field and numerical studies over a region of small hills, *Bulletin of the American Meteorological Society*, **92**, 1636–1650

Quenol, H. and Beltrando, G., 2008: Impact of a new railway line embankment (Mediterranean TGV) on the frequency of spring frosts in a fruit-growing area of the Durance Valley (South of France). *Meteorological Applications*, **15**, 389-398.

Riether, N., Rose, H., and Voigt, J., 1994: The KAMO cold-air model of the Umland-verband Frankfurt (UVF-Frankfurt and Environs Association). *Meteorologische Zeitschrift*, **N.F. 3**, 176-182.

Ryan A.P., 1975: Low level airflow patterns in Christchurch on nights of high air pollution potential. In: *Proceedings of the 8th Clean Air and Environment Conference, Rotorua, New Zealand*, 403–420.

Sachsen, T., Ketzler, G., Knörchen, A., and Schneider, C., 2013: Past and future evolution of nighttime urban cooling by suburban cold air drainage in Aachen. *Die Erde*, **144,** 274-289.

Salmond, J.A. and McKendry, I.G., 2005: Turbulence in the very stable nocturnal boundary layer: Implications for air pollution. *Progress in Physical Geograph*y, **29,** 171-188.

Schädler, G. and Lohmeyer, A., 1994: Simulation of nocturnal drainage flows on personal computers. *Meteorologische Zeitschrift*, **N.F. 3**, 167-171.

Schwab, A. and Zachenbacher, D., 2009: REKLIBO - Regionale Klimaanalyse Bodensee-Oberschwaben. Wissenschaftlicher *Abschlussbericht, Regionalverband-Bodensee-Oberschwaben*, **Band 1-4**. http://www.bodensee-oberschwaben.de/615_Projekte___Regionale_Klimaanalyse.RVBO

Sievers, U., 2005: Das Kaltluft-Abfluss-Modell KLAM_21. Grundlagen, Anwendungen und Handhabung des PC-Modells. *Berichte des Deutschen Wetterdienstes* **227**. Deutscher Wetterdienst, Offenbach a.M., Germany, 101 pp. http://nbn-resolving.de/urn:nbn:de:101:1-201207186729

Skyllingstad, E.D., 2003: Large-eddy simulation of katabatic flows. *Boundary-Layer Meteorology*, **106**, 217-243.

Spronken-Smith, R.A., Sturman, A.P., and Wilton, E.V., 2002: The air pollution problem in Christchurch, New Zealand – progress and prospects. *Clean Air and Environmental Quality*, **36**(1), 23-29.

Spronken-Smith, R.A., Kossmann, M, and Zawar-Reza, P., 2006: Where does all the energy go? Surface energy partitioning in suburban Christchurch under stable wintertime conditions. *Theor. Appl. Climatol.*, **84**, 137–149

Sturman, A.P., Fitzsimons, S.J., Holland, L.M., 1985: Local winds in the Southern Alps, New Zealand. *Journal of Climatology,* **5,** 145-160.

Sturman, A.P., Zawar-Reza, P., 2002: Application of back-trajectory techniques to the delimitation of urban clean air zones. *Atmospheric Environment,* **36**, 3339–3350.

Sun, J., Burns, S.P., Lenschow, D.H., Banta, R., Newsom, R., Coulter, R., Frasier, S., Ince, T., Nappo, C., Cuxart, J., Blumen, W., Lee, X., and Hu, X.-Z., 2002: Intermittent turbulence associated with a density current passage in the stable boundary layer. *Boundary-Layer Meteorology*, **105,** 199-219.

Sun, J., Burns, S.P., Delany, A.C., Oncley, S.P., Horst, T.W., and Lenschow, D.H., 2003: Heat balance in the nocturnal boundary layer during CASES-99. *Journal of Applied Meteorology*, **42,** 1649-1666.

Tate, A., Cullen, N.J., Spronken-Smith, R., 2011: Wintertime PM_{10} measurements and modelling in Alexandra, Central Otago, New Zealand: Understanding the bi-modal peak in evening air pollution. *Air Quality & Climate Change*, **45**(3), 19-25.

Titov, M., Sturman, A.P., Zawar-Reza, P., 2007: Application of MM5 and CAMx4 to local scale dispersion of particulate matter for the city of Christchurch, New Zealand. *Atmospheric Environment*, **41**, 327–338.

Trachte, K., Nauss, T., and Bendix, J., 2010: The Impact of different terrain configurations on the formation and dynamics of katabatic flows: Idealised case studies. *Boundary-Layer Meteorology*, **137**, 307-325.

VDI, 2003: *Environmental meteorology – Local cold air [Umweltmeteorologie – Lokale Kaltluft]*. VDI Guideline 3787/5. Beuth Verlag, Berlin.

Whiteman, C.D., 2000: *Mountain Meteorology – Fundamentals and Applications.* Kluwer Academic Publishers, Dordrecht.

Willmott, C.J. and Matsuura, K., 2005: Advantages of the mean absolute error (MAE) over the root mean square error (RMSE) in assessing average model performance. *Climate Research*, **30**, 79-82.

Wilson, J.G., Zawar-Reza, P., 2006: Intraurban-scale dispersion modelling of particulate matter concentrations: Applications for exposure estimates in cohort studies. *Atmospheric Environment*, **40**, 1053–1063.

Wratt, D.S., Salinger, M.J., Clarkson, T.S., Imrie, B.W., Bromley, A.M., Lechner, I.S., 1984: *Airflow and pollution dispersion in a valley - The Upper Hut Study*. New Zealand Meteorological Service, Scientific Report 4, Wellington New Zealand.

Zawar-Reza, P, Kingham, S., Pearce, J., 2005: Evaluation of a year-long dispersion modelling of PM_{10} using the mesoscale model TAPM for Christchurch, New Zealand. *Science of the Total Environment*, **349**, 249–259.

Zawar-Reza, P., Sturman, A.P., 2008: Application of airshed modelling to the implementation of the New Zealand National Environmental Standards for air quality. *Atmospheric Environment*, **42**, 8785–8794.

Appendix A: Parameterisation of surface and canopy friction

Vertical momentum exchange at the surface (term III_b in Eq. 5) is described through a friction coefficient c_*. For surface friction a logarithmic wind profile is assumed between the surface and the height of the wind speed maximum at $0.25\,H_{eff}$. This enables approximation of c_* from typical values of the aerodynamic roughness length z_0 (see Table 1) and the height of the wind speed maximum above ground through:

$$c_* = \left(\frac{2k}{\ln \frac{0.25 H_{eff}}{z_0}} \right)^2 \qquad \text{(A1)}$$

with the von Karman constant $k = 0.4$.

If in urban and forested areas the height of the wind speed maximum $0.25H_{eff}$ is less or equal the canopy height h, then the additional volume friction due to the canopy is modelled as unresolved obstacles through a porous medium approach (Gross, 1989) with c_* also depending on the canopy surface density σ:

$$c_* = \left(\frac{2k}{\ln \frac{0.25 H_{eff}}{z_0}} \right)^2 + c_d \, \sigma \, \alpha \, \min(H, h) \qquad \text{(A2)}$$

The drag coefficient c_d is set to the typical value of 0.2 (Gross, 1989) and the canopy surface density σ depends on the leaf or wall area index, the canopy height *h*, and the canopy surface cover fraction *b*.

In analogy to the well-known leaf area index *LAI*, the wall area index *WAI* is defined as the sum of the exterior building side walls per built surface area. The factor α depends on the wind speed profile. For $H<h$ and for $0.25H_{eff}=h$ the value of α equals 4/3. So for simplicity α is set to this value for all cases.

When the height of the wind speed maximum in urban or forested areas exceeds the canopy height, the concepts of

an effective roughness length $z_{0,\,eff}$ and a displacement height d are used to parameterise the friction coefficient:

$$c_* = \left(\frac{2k}{\ln \frac{0.25H_{eff} - d}{z_{0,\,eff}}} \right)^2 \qquad \text{(A3)}$$

When the height of the wind speed maximum $0.25H_{eff}$ is equal to the canopy height h, equations A3 and A2 should calculate the same magnitude of c_* to provide a steady transition between the two friction parameterisations, i.e.:

$$\left(\frac{2k}{\ln \frac{h-d}{z_{0,\,eff}}} \right)^2 = \left(\frac{2k}{\ln \frac{h}{z_0}} \right)^2 + \frac{4}{3} c_d \, \sigma \, h \qquad \text{(A4)}$$

Rearrangement of this equation can be used to determine the effective roughness length:

$$z_{0,\,eff} = (h-d)\exp(-\xi) \qquad \text{with} \qquad \text{(A5)}$$

$$\xi = \frac{k}{\sqrt{c_d \, \sigma \, h/3 + \left(\frac{k}{\ln \frac{h}{z_0}} \right)^2}} \qquad \text{(A6)}$$

The displacement height d is estimated empirically from the canopy height or obstacle height h and the fraction of surface area covered by the obstacles b:

$$d = 0.7\,h \, \min(1.0,\, 2b) \qquad \text{(A7)}$$

Appendix B: Parameterisation of ambient wind effects

KLAM_21 features the possibility to simulate the effects of a temporally constant ambient (regional) wind which interferes with the terrain induced drainage winds. While surface friction acts as a shear force from the bottom of the cold air, the regional wind represents a shear force from the top of the cold air layer. The regional wind shear force is calculated from the difference between wind vector $\vec{v}_{h,\,\max}$ at the height $0.25\,H_{eff}$ and the regional wind vector $\vec{v}_{reg}$ at the height h_{reg}, multiplied by a typical regional exchange coefficient for stable stratification $K_{m,reg}$ =1 m^2/s. The height h_{reg} at which the regional wind prevails depends empirically on a minimum height $h_{reg,0}$=40 m, the local cold air depth H, the local terrain height h_0, and on the maximum terrain height in the model domain $h_{0,\max}$:

$$h_{reg} = h_{reg,0} + \frac{h_{0,\max} + 3h_0}{4} + H \qquad \text{(A8)}$$

The regional wind term *REG* in equation 5 for the momentum budget of the cold air layer is given by:

$$REG = \frac{1}{H} \left(K_{m,reg} \frac{\vec{v}_{reg} - \vec{v}_{h,\max}}{h_{reg} - h_0 - 0.25H_{eff}} \right) \qquad \text{(A9)}$$

Appendix C: Dispersion of a passive tracer

The dispersion of a passive (inert) tracer emitted into the cold air layer can by simulated by KLAM_21. Assuming that all the tracer mass remains within the cold air layer (no sedimentation or deposition and no detrainment to the neutral residual layer aloft), the tendency of the vertically integrated tracer concentration C is given by:

$$\frac{\partial C}{\partial t} = -\nabla_h \cdot \frac{1}{\rho_0} \left\langle \rho_{eff} \, \vec{v}_h \right\rangle C + Q \qquad \text{(A10)}$$

Here Q is the mass of tracer emitted per surface area and time. The tracer concentration averaged vertically over the depth of the cold air layer is then calculated by:

$$c = \frac{C}{H} \tag{A11}$$

A specially formatted input file is used to define the location and strength of tracer sources in the model domain.

Submitted to *Weather and Climate Journal* 7 October 2015, revised 19 October 2016